Journal of Geophysical Research: Space Physics

RESEARCH ARTICLE
10.1029/2018JA025460

# Long-Lasting Response of the Global Thermosphere and Ionosphere to the 21 August 2017 Solar Eclipse

**Jiuhou Lei[1,2], Tong Dang[1], Wenbin Wang[3], Alan Burns[3], Binzheng Zhang[4,5], and Huijun Le[6,7,8]**

[1]CAS Key Laboratory of Geospace Environment, School of Earth and Space Sciences, University of Science and Technology of China, Hefei, China, [2]Mengcheng National Geophysical Observatory, University of Science and Technology of China, Hefei, China, [3]High Altitude Observatory, National Center for Atmospheric Research, Boulder, CO, USA, [4]Department of Earth Sciences, The University of Hong Kong, Pokfulam, Hong Kong, [5]Laboratory for Space Research, The University of Hong Kong, Pokfulam, Hong Kong, [6]Key Laboratory of Earth and Planetary Physics, Institute of Geology and Geophysics, Chinese Academy of Sciences, Beijing, China, [7]Institutions of Earth Science, Chinese Academy of Sciences, Beijing, China, [8]Geoscience School, University of the Chinese Academy of Sciences, Beijing, China

**Key Points:**
- This is the first quantitative analysis of the posteclipse response of the global ionosphere and thermosphere
- The posteclipse impact was found to persist for more than a half day after the eclipse

**Correspondence to:**
J. Lei,
leijh@ustc.edu.cn

**Citation:**
Lei, J., Dang, T., Wang, W., Burns, A., Zhang, B., & Le, H. (2018). Long-lasting response of the global thermosphere and ionosphere to the 21 August 2017 solar eclipse. *Journal of Geophysical Research: Space Physics*, *123*, 4309–4316. https://doi.org/10.1029/2018JA025460

Received 10 MAR 2018
Accepted 2 MAY 2018
Accepted article online 14 MAY 2018
Published online 24 MAY 2018

**Abstract** Previous studies have been devoted to examining the ionosphere and thermosphere response during the solar eclipse, but the posteclipse response of the global ionosphere and thermosphere has not been well quantified. In this study, for the first time, we quantitatively investigate the posteclipse response of the global ionosphere and thermosphere system to the recent Great American Solar Eclipse using a high-resolution, global, coupled ionosphere-thermosphere-electrodynamics model. It was found that the posteclipse response of the ionosphere and thermosphere is significant and worldwide, which was not expected. Specifically, even 9 hr after the eclipse ended, the globally averaged ionospheric total electron content perturbations were about 0.2 total electron content unit, and the corresponding changes in neutral temperature and winds reached 2 K and 2 m/s. The changes in the global dynamic and energetic processes associated with the solar eclipse contributed to this long-lasting response of the ionosphere and thermosphere during the posteclipse period.

**Plain Language Summary** The thermosphere is the layer of the Earth's atmosphere above the mesosphere between about 60 and 1,000 km, and the ionosphere is the ionized part of the atmosphere. In this region, the neutral gas and the ionized plasma have significant impact on low Earth orbiting determination and satellite radio communications. This work is the first to use a state-of-the-art, first-principles model of the coupled thermosphere and ionosphere, with self-consistent electrodynamics, to systematically investigate the dynamics and electrodynamic behavior of the global ionosphere and thermosphere after an eclipse. Although the solar eclipse is a transient local event, its impact on the ionosphere and thermosphere can persist for a long time over the entire globe, rather than just being an impulse event with a localized response as was previously expected. This effort paves the way for improving the understanding of the upper atmospheric variability.

## 1. Introduction

The ionospheric response to solar eclipses has been widely studied using various observations such as those by ionosondes, incoherent scatter radars, the global positioning system, and satellite measurements (Anastassiadis & Matsoukas, 1969; Davis et al., 2000; Ding et al., 2010; Farges et al., 2001; Le et al., 2009; Salah et al., 1986), as well as numerical simulations (Müller-Wodarg et al., 1998; Ridley et al., 1984; Roble et al., 1986). These studies showed that there is a significant depletion in the ionosphere during the eclipse, due to the rapid reduction of the solar EUV irradiation.

Besides the ionosphere responses during the eclipse period, some attention has been paid to the posteclipse effects of the ionosphere within the shadow region. The posteclipse response of the ionosphere has altitudinal dependence, with a faster recovery in the $E$ and $F_1$ regions, and a slower one in the $F_2$ region (Adeniyi et al., 2007; Le et al., 2008a, 2008b; Rishbeth, 1963). Observations have also indicated that the ionosphere and thermosphere during the posteclipse period could have responses in regions far away from the Moon's shadow (e.g., Tsai & Liu, 1999). However, the ionospheric day-to-day variability is large; thus, the post-eclipse effects in the ionosphere are greatly masked and are difficult to isolate from observational data sets.

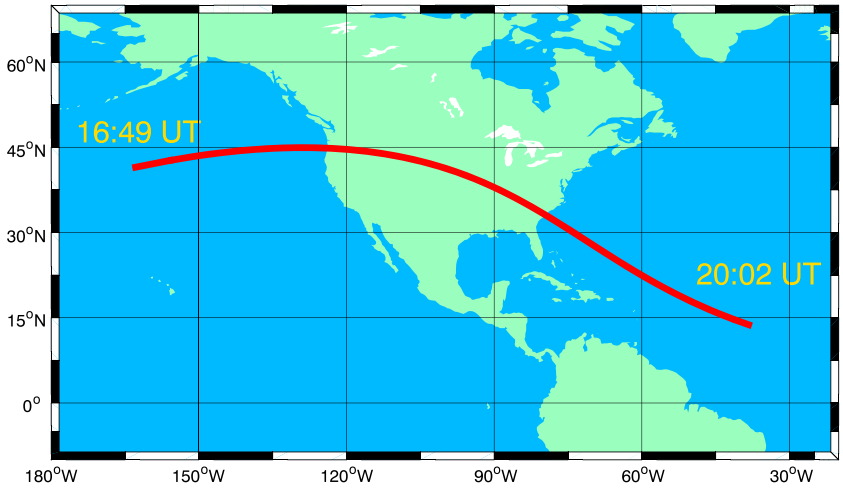


**Figure 1.** Totality path of the 21 August 2017 solar eclipse. The totality path began at 16:49 UT and ended at 20:02 UT. The penumbral shadow of the solar eclipse disappeared at 21:04 UT on 21 August.

As a consequence of these difficulties, the posteclipse response of the ionosphere and thermosphere is poorly understood and cannot be quantified using observations only.

In order to understand what the above-mentioned changes due to posteclipse response are, how they are likely to be seen in the data and what are the physical mechanisms driving these changes, it is thus necessary to investigate them first using controlled numerical experiments from a first-principles physics-based model, and then apply this knowledge to facilitate the understanding of observations. To this end, we explore the global response of the ionosphere-thermosphere (I-T) system during the postperiod of the 21 August 2017 eclipse, utilizing the high-resolution version of the Thermosphere Ionosphere Electrodynamics General Circulation Model (TIEGCM). This numerical study focused on the posteclipse response provides new insights for future eclipse event-based studies of the coupled I-T system, both theoretical and observational.

## 2. Methodology

The TIEGCM is a time-dependent, self-consistent, three-dimensional, and physics-based model of the global thermosphere/ionosphere system (Richmond et al., 1992; Roble et al., 1988). The horizontal resolution used in this study is 0.625° × 0.625° in a geographic latitude-longitude grid with a vertical resolution of one fourth of a scale height. In this study, the convection pattern at high latitudes is specified by the Heelis model (Heelis et al., 1982), which is driven by the geomagnetic activity index Kp. We drove the TIEGCM with a fixed Kp value of 0.1 to minimize the influence of geomagnetic activity.

The solar eclipse on 21 August 2017, which is also referred to as the Great American Solar Eclipse, crossed the center of the continental United States from the Pacific to the Atlantic Oceans (Figure 1). The Moon's shadow first touched the Earth at 15:47 UT over the Pacific Ocean. The total eclipse began at 16:49 UT over the east Pacific Ocean, and it ended over the North Atlantic Ocean at 20:02 UT. The penumbral shadow of the solar eclipse disappeared at 21:04 UT on 21 August. As the solar eclipse occurs, the solar radiation flux is multiplied by an eclipse factor function, which is calculated based on the ratio that the Sun is masked by the Moon during the eclipse. The treatment of the eclipse factor function in the TIEGCM is based on the studies of Curto et al. (2006) and Le et al. (2008b). More details about the methodology can be found in the Dang et al. (2018). We conducted two TIEGCM simulations: one with, and the other without, the solar eclipse effect. The differential fields between these two simulations are used here to explore the solar eclipse impact on the global ionosphere and thermosphere.

## 3. Results and Discussion

Figure 2 shows global maps of the differences between the TIEGCM simulations with and without the eclipse of total electron content (TEC), neutral temperature, meridional winds, and vertical plasma drifts at 06:00 UT

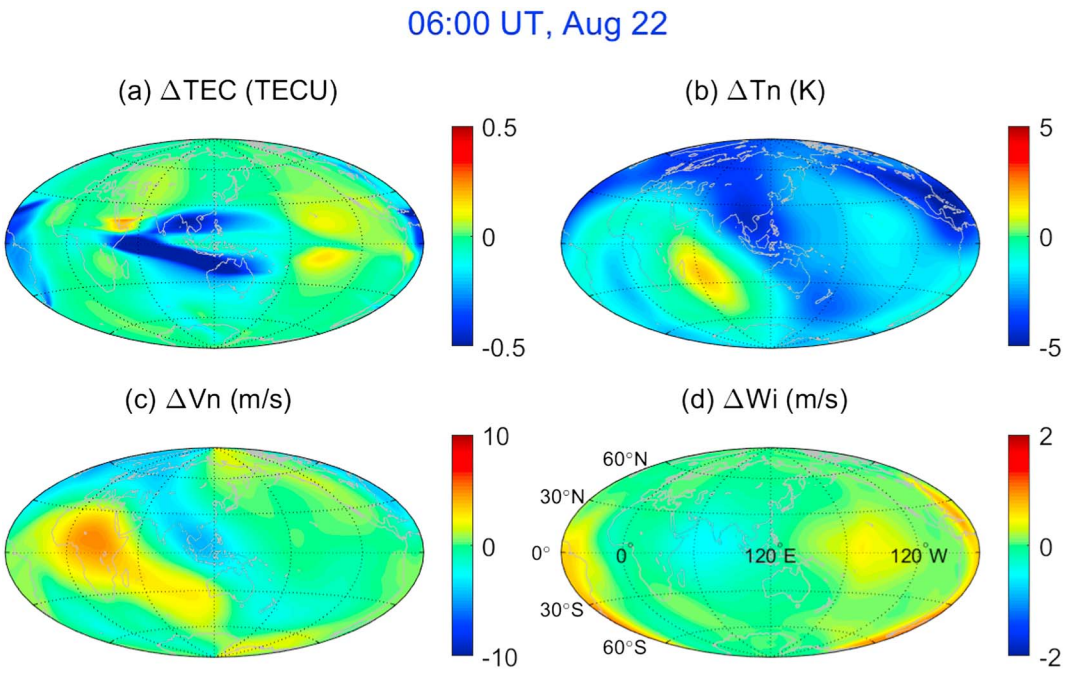


**Figure 2.** Global maps of differential TEC, neutral temperature, meridional winds (northward positive), and $E \times B$ vertical plasma drifts (upward positive) at pressure level 2 (~300 km) between the TIEGCM simulations with and without eclipse (with eclipse-without eclipse) at 06:00 UT on 22 August 2017, 9 hr after the eclipse ended.

on 22 August 2017, the day after the eclipse. In Figure 2a, two stripes of TEC depletions occurred in the Asia sector at low latitudes near the equatorial ionization anomaly (EIA) regions: one was located over South Asia between 60°E and 60°W and the other one stretched from Africa near the equator all the way to Australia. The TEC has a maximum depletion of around 0.5 TEC units (TECU; 1 TECU = $10^{16}$/m$^2$) at 06:00 UT. It is interesting to note that although the solar eclipse had ended about 9 hr earlier, TEC depletions still existed over North America and the west of the Atlantic Ocean. Near the longitude of 150°W, the TEC enhancement was seen at latitudes of about ±15°, with a magnitude of 0.2 TECU. Both TEC increases and decreases may be associated with perturbations of plasma drifts. Although these TEC changes during the posteclipse period are not huge, they are much greater than those due to bow waves and to gravity waves with periods of 10–30 min (Nayak & Yiğit, 2018; Zhang et al., 2017).

As shown in Figure 2, at 06:00 UT on 22 August 2017, the thermospheric perturbations induced by the solar eclipse had not disappeared. The neutral temperature in Figure 2b has a depletion of about 5 K in a broad area including the Asian, Oceania and American sectors. A temperature increase occurred over the southeastern side of Africa, with a magnitude of about 3 K. The meridional winds in Figure 2c had northward perturbations at Africa and southward perturbations in the Asian sector with a maximum magnitude of about 5 m/s.

Figure 2d shows the changes in ionospheric electric fields at 06:00 UT, as represented by the vertical plasma $E \times B$ drift perturbations. At low latitudes, and in the equatorial region, downward plasma drifts occurred at longitudes between 40°E and 120°E, whereas upward plasma drifts existed near 160°W over the Pacific Ocean. These downward and upward plasma drifts were most likely responsible for the TEC changes in the EIA region in Figure 2a. The upward plasma drifts tend to intensify the EIA crests, whereas the downward ones suppress the equatorial fountain effect and consequently contribute to the TEC depletion in the EIA region at longitudes between 40°E and 120°E. Over the America and West Africa, at low and middle latitudes, there were also vertical plasma drift perturbations. Note that Figure 2d is just a snap shot of the changes of vertical plasma drifts at 06:00 UT, whereas the TEC changes in Figure 2a represent the time-integrated effects of vertical drifts, as well as other potential contributors such as neutral winds and composition, on ionospheric plasma density. Thus, the global structures of TEC changes may not be exactly match the patterns of vertical drift changes observed simultaneously. Huba and Drob (2017) and Dang et al. (2018)

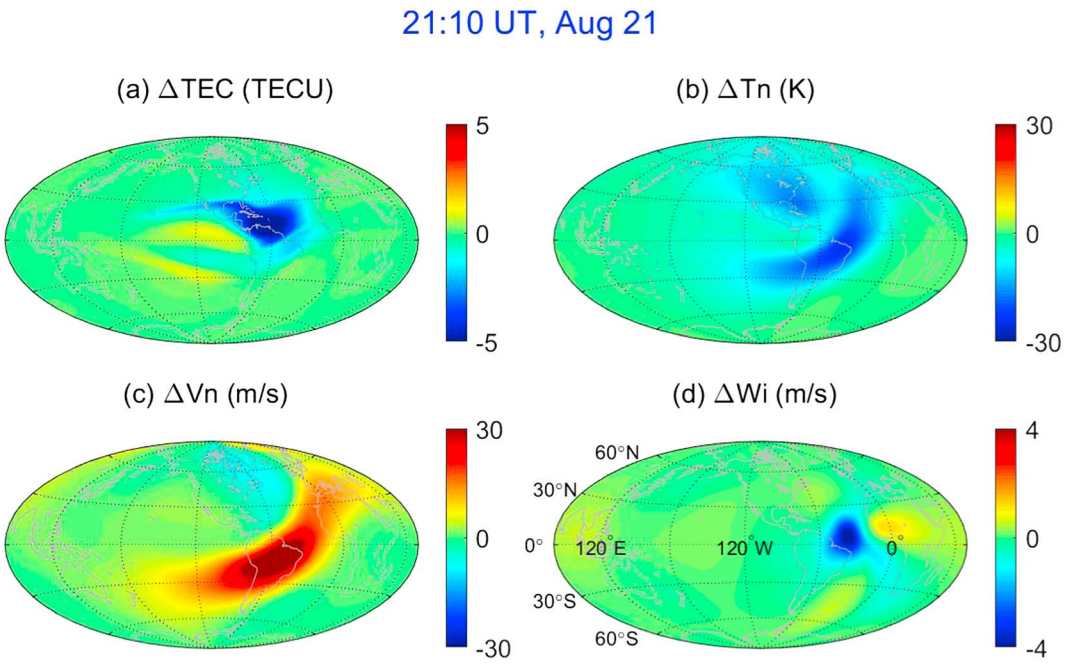


**Figure 3.** Same as Figure 2 but at 21:10 UT on 21 August 2017 when the solar eclipse just ended.

indicated that electrodynamic processes play a critical role in the global response of the I-T system to the solar eclipse. Associated with thermospheric wind changes and *E* region and *F* region dynamo effects, ionospheric electric fields exhibited long and continuous global perturbations. Nine hours after the eclipse had ended, the maximum magnitudes were about 5 m/s in the changes of meridional winds and 1 m/s in vertical plasma drift changes, which could further influence the recovery of the TEC perturbations caused by the solar eclipse.

Figure 3 shows similar plots as Figure 2 but for the snap shots of the changes of TEC, neutral temperature, meridional winds, and vertical plasma drifts at 21:10 UT on 21 August. This is the time when the lunar screening was just completely gone. The comparison between the results in Figures 2 and 3 serves as a reference to observe the evolution of posteclipse effects. As shown in Figure 3a, the TEC has a depletion of 5 TEC over the Central America. Besides the visible perturbations over the east-south of the North America, which were associated with the Moon shadow, both neutral temperature and meridional winds in Figures 3b and 3c showed large-scale traveling atmospheric disturbances (TADs), with a perturbation of 30 m/s and 40 K, respectively. The large-scale TADs propagated globally, induced global ionospheric and thermospheric changes, and contributed to the long recovery of the ionosphere and thermosphere. The plasma drifts associated with the electrodynamic processes in Figure 3d exhibited a downward perturbation near the east coast of the South America and an upward perturbation over the West Africa. This strong downward drift perturbation could be responsible for the TEC depletion seen in Figure 3a. However, the hemispherically asymmetric depletion of the TEC in the America sector could be associated with wind transport effects, which tend to reduce the TEC depletion in the southern hemisphere. Overall, the ionospheric and thermospheric perturbations in Figure 3 were much larger than those seen in Figure 2, 9 hr later after the eclipse ended. This is expected since the themosphere and ionosphere have had a long time to recover. Nevertheless, the simulation results indicate that the thermosphere-ionosphere system has a long-lasting response to the solar eclipse.

In order to quantitatively examine the posteclipse response of the global I-T system to the solar eclipse, we computed the globally area-averaged standard deviations (SDs) of the difference between TIEGCM simulations with and without eclipse for TEC, $F_2$-region peak electron density (NmF2), neutral temperature, meridional and zonal winds, and vertical plasma drifts from 15 UT on 21 August to 12 UT on 22 August. Note that the calculated SDs represent the averaged magnitude of the eclipsed-induced perturbations in

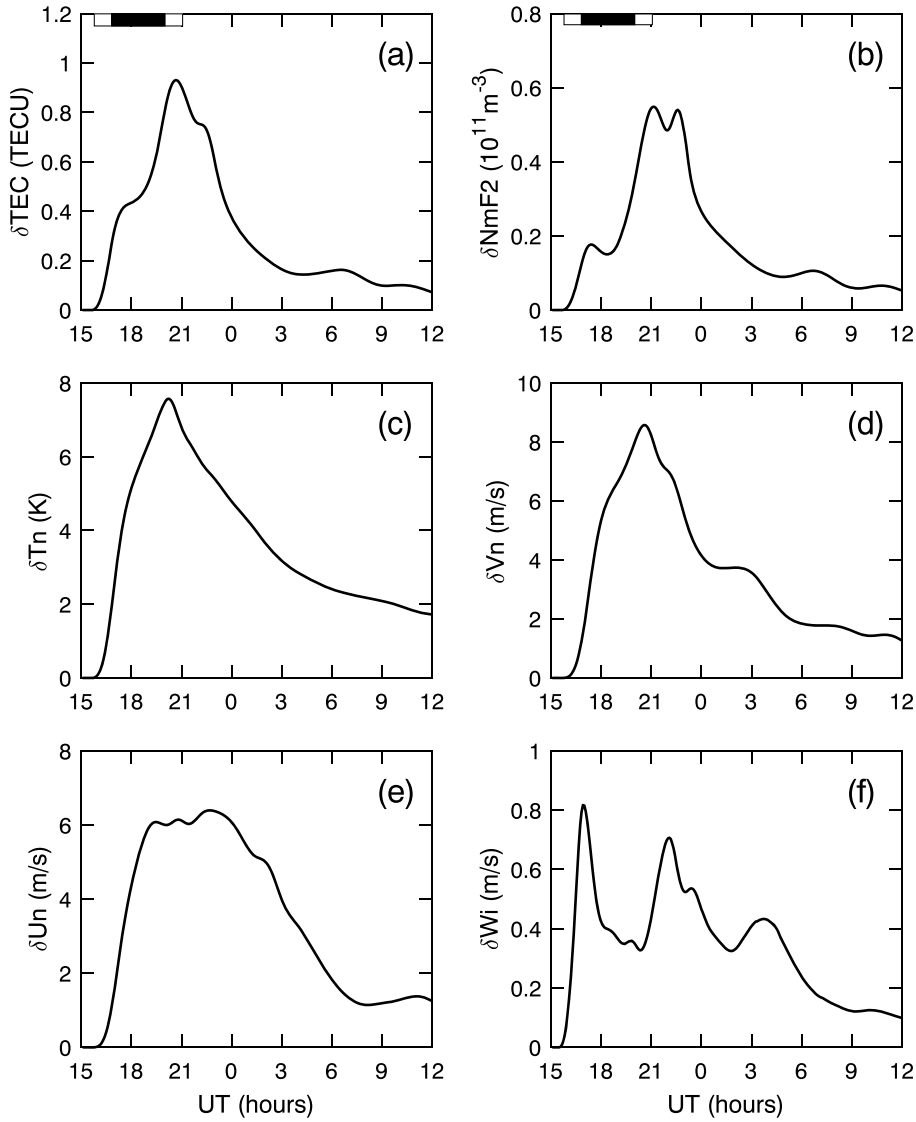


**Figure 4.** The globally area averaged standard deviations calculated from the difference between the TIEGCM simulations with and without the eclipse for (a) TEC, (b) NmF2, (c) neutral temperature, (d) meridional winds (positive northward), (e) zonal winds (positive eastward), and (f) vertical plasma drifts (positive upward) from 15 UT on 21 August to 12 UT on 22 August. The black and white bars in the upper panels indicate the duration of umbra (total eclipse) and penumbra (partial eclipse), respectively.

the whole globe, which can be much less than the actual changes in the ionosphere and thermosphere for a specific local region.

As shown in Figure 4a, the TEC SD started to increase at about 15:50 UT when the partial eclipse first touched the Earth. The TEC SD maximized at around 21:00 UT, with a magnitude of 1 TECU. This was the time when the eclipse ended and the Moon's shadow entirely left the Earth. After that, the TEC SD began to decrease. The TEC SD still had a magnitude of about 0.2 TECU at 06:00 UT, and then the TEC SD only declined slightly. Thus, global TEC appears to take more than a half day to recover to near-pre-eclipse conditions. Note that TEC SD at 06:00 UT is about 0.2 TECU, but the TEC changes can be larger than 0.5 TECU in some regions (Figure 2a). The variation of NmF2 SD in Figure 4b was similar to TEC SD, but with a larger second peak at around 23:00 UT, about 2 hr after the eclipse had ended.

The SD variations of thermospheric temperature, meridional and zonal winds, and the vertical plasma drifts are plotted in Figures 4c–4f at a pressure level of 2, which is close to the peak altitude of the $F_2$ region. The

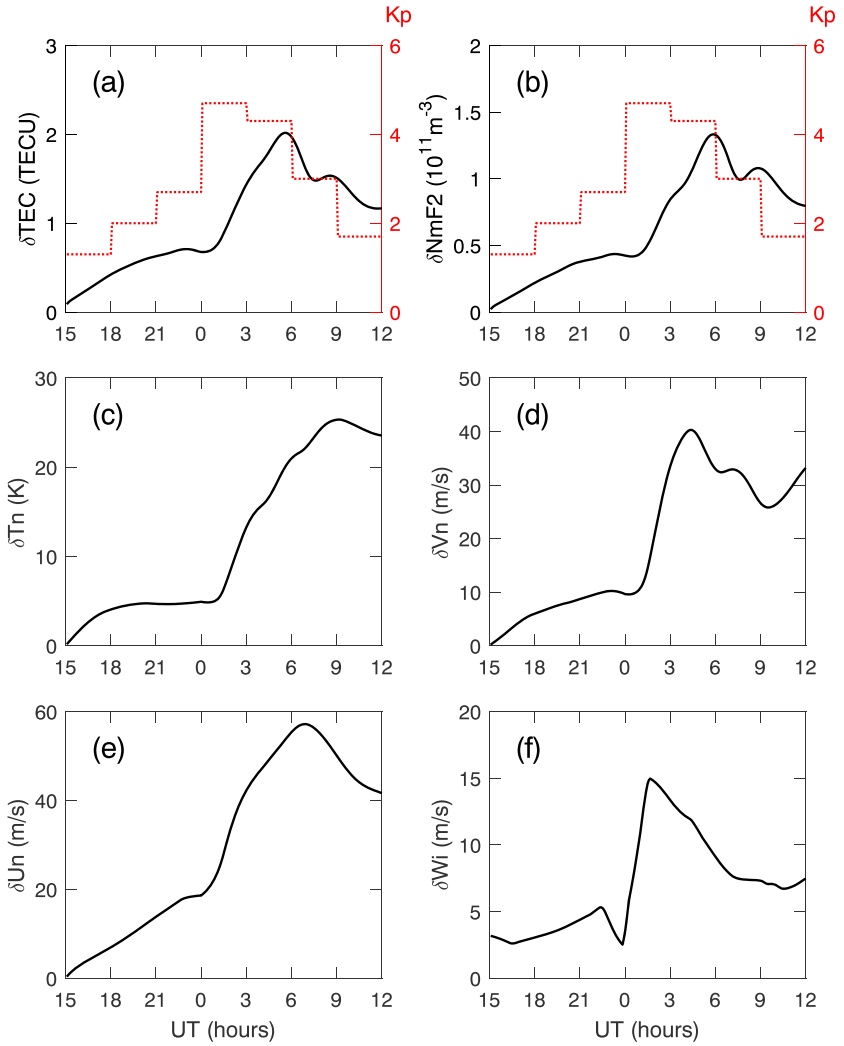


**Figure 5.** Evolution of the averaged standard deviations from the difference between the two TIEGCM simulations without the solar eclipse effects: one driven by the actual Kp values and the other with a fixed Kp value of 0.1. The shown parameters include (a) TEC, (b) NmF2, (c) neutral temperature, (d) meridional winds (positive northward), (e) zonal winds (positive eastward), and (f) vertical plasma drifts (positive upward) in the period from 15 UT on 21 August to 12 UT on 22 August. In this figure we showed the weighted results within the latitudes of 60°, given that the electric field variability during the geomagnetic disturbance in the polar region depends on the imposed convection from the empirical model. The red dashed bars represent the actual values of the Kp index during the period.

thermospheric temperature SD has a similar variation to the TEC SD; however, it has a slower recovery than the TEC SD. At 06:00 UT on 22 August, there was still a temperature SD of 2.4 K, which is around one third of the maximum value. The SD variations of meridional and zonal winds with time were generally consistent with that of the thermospheric temperature. The SDs in both meridional winds and zonal winds increased when the eclipse touched the Earth, attained maximums during the eclipse, and then decreased to about 2 m/s at 06:00 UT. The major differences between zonal and meridional winds are the second peak of zonal winds SD at about 00:00 UT. The differences between the global perturbations of zonal and meridional winds were related to the propagation of the large-scale TADs.

The variation of vertical plasma drift SD in Figure 4f is different from other parameters. Note that if a full plasmasphere, for example, SAMI3 (Huba & Drob, 2017), is included in the TIEGCM, it could only have small influences on the plasma drift variations as the electron densities in the plasmasphere are much lower than those in the *E* and *F* region ionosphere and contribute negligibly to the ionospheric conductance. The plasma drift

SD peaked at about 17:00 UT with a velocity of 0.8 m/s and then rapidly dropped to a speed less than 0.4 m/s. The SD of plasma drift variations exhibited oscillations during the recovery after the eclipse ended, especially between 21:00 UT and 24:00 UT on 21 August. These oscillations were most likely associated with the TADs. The SD of plasma drifts had a speed of about 0.2 m/s at 06:00 UT on 22 August. As discussed later, the global perturbations of vertical plasma drifts are caused by the ionospheric dynamo effect associated with disturbance winds.

In order to illustrate the day-to-day variability of the ionosphere and thermosphere associated with geomagnetic activity, we conducted an additional model simulation driven by the actual geomagnetic activity from 15 UT on 21 August, but without the solar eclipse effect. The differential fields between the two simulations without solar eclipse (one driven by the actual geomagnetic activity and the other by a fixed Kp value of 0.1) are shown in Figure 5. It is clear that ionospheric and thermospheric variability depends on geomagnetic activity and preconditioning. On 22 August when Kp reached 5 and a moderate storm occurred, the SDs for both ionospheric and thermospheric parameters generally were larger than those due to the solar eclipse. However, before that, the simulated ionospheric and thermospheric variability due to the solar eclipse is comparable to that seen from a typical quiet time geomagnetic activity period (Kp = 1~3), especially for the TEC and NmF2. Therefore, the ionospheric and thermospheric changes associated with the posteclipse effects are not negligible.

The results in Figure 4 above indicate that the global I-T system needs a long time to recover back to its unperturbed state. Even 15 hr after the eclipse ended, the ionospheric and thermospheric parameters have not gone back to preeclipse condition levels. It is generally believed that the solar eclipse simply impacts the ionosphere and thermosphere by reducing the EUV ionization and energy input to the upper atmosphere. Our study has shown that the solar eclipse, which has some characteristics that are similar to geomagnetic storm, has global and complicated influences through dynamic and electrodynamic coupling between the ionosphere and the thermosphere. Large-scale TADs, as seen in the thermospheric temperature and winds, were triggered during the solar eclipse and propagated northward and southward over the globe. The propagation of large-scale TADs leads to the perturbations of the global thermosphere and also its slow recovery, which is indicated in the SD variations of the perturbations of thermospheric temperature and winds in Figures 4c–4e. At the same time, the perturbations of the thermosphere can further modulate electron density and TEC distributions, and vice versa.

On the other hand, the ionosphere and thermosphere are also tightly coupled via electrodynamic processes. Neutral wind perturbations can lead to changes in electric field/plasma drifts, mainly through the *E* and *F* region dynamo effects. As seen in Figure 3f, the vertical plasma drifts strongly responded at the beginning of the solar eclipse. We further checked the simulation results and found that these strong plasma drifts mainly occurred in the longitudinal zone over the Pacific Ocean. This feature is interesting and the underlying mechanism needs further investigation, but it is beyond the scope of this posteclipse study. The global SD of vertical plasma drifts had long and persistent perturbations after the eclipse ended, indicating that there were perturbations in electric fields and vertical drifts after the eclipse to contribute to the long recovery of the global electron density and TEC distributions.

It should be noted that the long-lasting response of the ionosphere could also be associated with the totality trajectory of the solar eclipse. As shown in Figure 1, this solar eclipse, which crossed the entire North American continent, started over the Pacific Ocean, traversed the middle latitudes over the Americas, and ended over the North Atlantic Ocean, in the low latitudes. Thus, the ionosphere and thermosphere were disturbed in a large latitudinal range associated with the track of the solar eclipse. The induced ionosphere and thermosphere perturbations during the posteclipse could also depend on season, as well as whether the solar eclipse is an annular or total one (Roble et al., 1986). Thus, the characteristics of the posteclipse response in the ionosphere and thermosphere should vary from one solar eclipse to another. As mentioned earlier, it is a great challenge to isolate the ionospheric and thermospheric variability solely induced by the solar eclipse from the observations, as other geophysical changes can conceal eclipse effects. Thus, It is worth noting that geomagnetic activity and the lower atmosphere forcing can further modulate the posteclipse variability of the ionosphere and thermosphere. Nevertheless, our study provides an important baseline for the posteclipse response of the global ionosphere and thermosphere, albeit further investigations are needed using both data and a whole atmospheric model, for example, the Whole Atmosphere Community Climate Model with thermosphere and ionosphere extension (Liu et al., 2018).

## 4. Summary

In this study, we quantify the posteclipse response of the global I-T system to the recent Great American Solar Eclipse using a high-resolution coupled ionosphere-thermosphere-electrodynamics model. The ionosphere and thermosphere showed significant changes globally even after the eclipse had been over for more than a half day. The persistent perturbations of thermospheric winds and temperatures and the resultant electrodynamic changes associated with the global dynamic and energetic processes contributed to the long-lasting response of ionospheric electron density and TEC. Therefore, although the solar eclipse is a transient local event, its impact on the ionosphere and thermosphere can persist for a long time over the entire globe, rather than just being an impulse event with a localized response as was previously expected.

**Acknowledgments**
This work was supported by the National Natural Science Foundation of China (41325017 and 41421063), the Opening Funding of Chinese Academy of Sciences dedicated for the Chinese Meridian Project, and the Thousand Young Talents Program of China. The National Center for Atmospheric Research is sponsored by the National Science Foundation. We would like to acknowledge high-performance computing support from Cheyenne (doi:10.5065/D6RX99HX) provided by NCAR's Computational and Information Systems Laboratory, sponsored by the National Science Foundation (NSF). Model output data are archived on the NCAR High Performance Storage System (HPSS).

## References

Adeniyi, J. O., Radicella, S. M., Adimula, I. A., Willoughby, A. A., Oladipo, O. A., & Olawepo, O. (2007). Signature of the 29 March 2006 eclipse on the ionosphere over an equatorial station. *Journal of Geophysical Research*, *112*, A06314. https://doi.org/10.1029/2006JA012197

Anastassiadis, M., & Matsoukas, D. (1969). Electron content measurements by beacon S-66 satellite during the May 20, 1966, solar eclipse. *Journal of Atmospheric and Terrestrial Physics*, *31*(9), 1217–1222. https://doi.org/10.1016/0021-9169(69)90056-7

Curto, J. J., Heilig, B., & Piñol, M. (2006). Modeling the geomagnetic effects caused by the solar eclipse of 11 August 1999. *Journal of Geophysical Research*, *111*, A07312. https://doi.org/10.1029/2005JA011499

Dang, T., Lei, J., Wang, W., Burns, A., Zhang, B., & Zhang, S. R. (2018). Suppression of the polar tongue of ionization during the 21 August 2017 solar eclipse. *Geophysical Research Letters*, *45*, 2918–2925. https://doi.org/10.1002/2018GL077328

Davis, C. J., Lockwood, M., Bell, S. A., Smith, J. A., & Clarke, E. M. (2000). Ionospheric measurements of relative coronal brightness during the total solar eclipses of 11 August, 1999 and 9 July, 1945. *Annales de Geophysique*, *18*(2), 182–190. https://doi.org/10.1007/s00585-000-0182-z

Ding, F., Wan, W., Ning, B., Liu, L., Le, H., Xu, G., et al. (2010). GPS TEC response to the 22 July 2009 total solar eclipse in East Asia. *Journal of Geophysical Research*, *115*, A07308. https://doi.org/10.1029/2009JA015113

Farges, T., Jodogne, J. C., Bamford, R., Le Roux, Y., Gauthier, F., Vila, P. M., et al. (2001). Disturbances of the western European ionosphere during the total solar eclipse of 11 August 1999 measured by a wide ionosonde and radar network. *Journal of Atmospheric and Solar - Terrestrial Physics*, *63*(9), 915–924. https://doi.org/10.1016/S1364-6826(00)00195-4

Heelis, R. A., Lowell, J. K., & Spiro, R. W. (1982). A model of the high-latitude ionospheric convection pattern. *Journal of Geophysical Research*, *87*(A8), 6339–6345. https://doi.org/10.1029/JA087iA08p06339

Huba, J. D., & Drob, D. (2017). SAMI3 prediction of the impact of the 21 August 2017 total solar eclipse on the ionosphere/plasmasphere system. *Geophysical Research Letters*, *44*, 5928–5935. https://doi.org/10.1002/2017GL073549

Le, H., Liu, L., Yue, X., & Wan, W. (2008a). The ionospheric responses to the 11 August 1999 solar eclipse: Observations and modeling. *Annales de Geophysique*, *26*(1), 107–116. https://doi.org/10.5194/angeo-26-107-2008

Le, H., Liu, L., Yue, X., & Wan, W. (2008b). The midlatitude $F_2$ layer during solar eclipses: Observations and modeling. *Journal of Geophysical Research*, *113*, A08309. https://doi.org/10.1029/2007JA013012

Le, H., Liu, L., Yue, X., Wan, W., & Ning, B. (2009). Latitudinal dependence of the ionospheric response to solar eclipses. *Journal of Geophysical Research*, *114*, A07308. https://doi.org/10.1029/2009JA014072

Liu, H.-L., Bardeen, C. G., Foster, B. T., Lauritzen, P., Liu, J., Lu, G., et al. (2018). Development and validation of the Whole Atmosphere Community Climate Model with thermosphere and ionosphere extension (WACCM-X 2.0). *Journal of Advances in Modeling Earth Systems*, *10*, 381–402. https://doi.org/10.1002/2017MS001232

Müller-Wodarg, I. C. F., Aylward, A. D., & Lockwood, M. (1998). Effects of a mid-latitude solar eclipse on the thermosphere and ionosphere—A modelling study. *Geophysical Research Letters*, *25*(20), 3787–3790. https://doi.org/10.1029/1998GL900045

Nayak, C., & Yiğit, E. (2018). GPS-TEC observation of gravity waves generated in the ionosphere during 21 August 2017 total solar eclipse. *Journal of Geophysical Research*, *123*, 725–738. https://doi.org/10.1002/2017JA024845

Richmond, A. D., Ridley, E. C., & Roble, R. G. (1992). A thermosphere/ionosphere general circulation model with coupled electrodynamics. *Geophysical Research Letters*, *19*(6), 601–604. https://doi.org/10.1029/92GL00401

Ridley, E. C., Dickinson, R. E., Roble, R. G., & Rees, M. H. (1984). Thermospheric response to the June 11, 1983, solar eclipse. *Journal of Geophysical Research*, *89*(A9), 7583–7588. https://doi.org/10.1029/JA089iA09p07583

Rishbeth, H. (1963). Further analogue studies of the ionospheric *F* layer. *Proceedings of the Physical Society*, *81*(1), 65–77. https://doi.org/10.1088/0370-1328/81/1/312

Roble, R. G., Emery, B. A., & Ridley, E. C. (1986). Ionospheric and thermospheric response over Millstone Hill to the May 30, 1984, annular solar eclipse. *Journal of Geophysical Research*, *91*(A2), 1661–1670. https://doi.org/10.1029/JA091iA02p01661

Roble, R. G., Ridley, E. C., Richmond, A. D., & Dickinson, R. E. (1988). A coupled thermosphere/ionosphere general circulation model. *Geophysical Research Letters*, *15*(12), 1325–1328. https://doi.org/10.1029/GL015i012p01325

Salah, J. E., Oliver, W. L., Foster, J. C., Holt, J. M., Emery, B. A., & Roble, R. G. (1986). Observations of the May 30, 1984, annular solar eclipse at Millstone Hill. *Journal of Geophysical Research*, *91*(A2), 1651–1660. https://doi.org/10.1029/JA091iA02p01651

Tsai, H. F., & Liu, J. Y. (1999). Ionospheric total electron content response to solar eclipses. *Journal of Geophysical Research*, *104*(A6), 12,657–12,668. https://doi.org/10.1029/1999JA900001

Zhang, S.-R., Erickson, P. J., Goncharenko, L. P., Coster, A. J., Rideout, W., & Vierinen, J. (2017). Ionospheric bow waves and perturbations induced by the 21 August 2017 solar eclipse. *Geophysical Research Letters*, *44*, 12,067–12,073. https://doi.org/10.1002/2017GL076054